

Atomic Physics with Accelerators:
Projectile Electron Spectroscopy
Work Package 9

Analysis and presentation of new results

Project Coordinator:
Prof. Theo Zouros

Editors:
Madesis Ioannis
imadesis@physics.uoc.gr

<http://apapes.physics.uoc.gr>

Contributors:
Prof. Theo Zouros - MRG RT1 (UoC)
Ioannis Madesis (Ph.D. student) - GEC RT1 (UoC)
Dr. Anastasios Dimitriou (postdoc) - GEC RT1 (UoC)
Prof. Emmanouil Benis - MRG RT3 (UoI)
Dr. Bela Sulik - MRG RT1 (ATOMKI, Debrecen Hungary)
Angelos Laoutaris (M.Sc. student) - GEC RT1 (UoC)
Prof. Omer Sise (Suleyman Demirel University) - GEC RT1 (UoC)

30/11/2015

Contents

1	Introduction	1
2	Data Analysis: From raw DAQ files to final results	1
2.1	Energy Calibration	2
2.2	Laboratory to Rest frame Energy transformation	4
2.3	Normalization	4
3	Data analysis	7
3.1	Homebuilt Software	7
3.1.1	Self Energy Calibrating Excel	7
3.1.2	Optimal Slit settings Excel	7
3.1.3	Spectrograph voltage Excel	8
3.1.4	Various other control programs	8
3.2	Results using SIMION software	8
3.2.1	Experimental energy resolution of a paracentric hemispherical deflector analyzer for different entry positions and bias	8
3.2.2	Determination of the solid angle and response function of a hemispherical spectrograph with injection lens for Auger electrons emitted from long lived projectile states	9
3.2.3	The Optimization of a 4-Element Input Lens on a Hemispherical Deflector Analyzer Using SIMION	9
3.2.4	Voltage optimization of a 4-element injection lens on a hemispherical spectrograph with virtual entry aperture	9
3.2.5	Evaluation of the effective solid angle of a hemispherical deflector analyser with injection lens for metastable Auger projectile states	10
4	Presentation of new results	10
4.1	Capture ratio R	10
4.2	Biased gas cell measurements	10
5	Concluding Remarks	11

List of Figures

1	Ratio R	11
---	---------------------	----

1 Introduction

Work Package 9 Technical Report details the analysis and presentation of the results of the APAPES project to date. In the first part, we present the procedures followed to convert the raw data from the DAQ into the final spectrum of each measurement, along with further details.

2 Data Analysis: From raw DAQ files to final results

As already presented, the apparatus includes a 2-D PSD which together with the DAQ software generates files that have the specific information of every cell in the 2-D matrix representing the PSD information. Our choice was to mostly use either the 256×256 presentation as used before [1] or when needed a 512×512 representation allowing more detailed information about the spectra but taking more time. All collected data with same X-coordinate¹ or Y-coordinate were summed to a triple column “projection file”. The user selects a rectangular area on the PSD image online for X-projections and one for Y-projections. By careful placement of these rectangles, much of the unwanted background can be filtered. The final data consists of the columns: 1) channel number, 2) summation for the same “Y” channels, 3) summation for same “X” (energy) channels, always in the selected rectangles.

The analysis of any spectrum acquired with the ZAPS method requires the following distinctive steps before it can be performed:

1. **Background subtraction.** A mostly quadratic background (BKG) was fit to the spectra and subtracted.
2. **Energy Calibration.** Each spectrum acquired needs to be energy calibrated. A quadratic function of the “X” channel of the detector was assigned to the laboratory electron energy in eV.
3. **Lab-to-rest frame transformation.** The lab electron energies were transformed to the rest frame of the projectile ion using mostly relativistic transformation formulas [2] for higher accuracy.
4. **Normalization.** The final step for every spectrum is to be normalized either in a relative or absolute way to eventually obtain normalized yields or even double differential cross sections in energy and solid angle as detailed in the following sections.

For the needs of the APAPES project, a special excel file was constructed, that performs all the above tasks and is constantly updated. The

¹bins of same energy

main advantage of this file is that it requires only 3 specific inputs: The spectrum, the experimental conditions and the constants of the fitted functions on the raw data. It is explained in detail in section 3.1.

2.1 Energy Calibration

In general, this is not a trivial procedure, because the energy of the measured electrons depends highly on the projectile energy. Although the energies of the KLL Auger electrons are mostly well known and can be used for calibration, the precise projectile energy at each beam time is not known accurately enough. A 1% error in beam energy can lead to an error of 0.6 %, or about 0.9 eV in the case of Carbon *KLL* from a 12 MeV beam. However, the energy error in the beam is in the range of 0.1% error which is relatively small (but not negligible). Using known Auger energies (we used the Carbon KLL values mostly listed in Bruch et al. [3]) which appeared in the spectrum itself, the spectrum was self-calibrated. By combining the data that resulted from the fitting procedure with the known peaks transformed in the lab frame, the Excel file automatically generates the necessary three a,b,c constants by Least Squares Method

$$T(i) = a + b \cdot i + c \cdot i^2 \quad (2.1)$$

This leads to a direct quadratic function that assigns a value for lab frame energy T to every “X” channel number i . The procedure is rather simple. Since the Auger energies and the projectile energy are known, the first step is to transform the Auger energies (rest frame electron energy) to the lab frame.

Rest frame to Laboratory Energy transformation

Auger electrons emitted from scattered projectiles are kinematically influenced. A detailed analysis of the general electron kinematic effects can be quite complicated [4, 5]. However, for the case of energetic collisions of a few MeV/u or larger, projectile ions are scattered through very small angles (\sim mrad), resulting in negligible effects both on the energy loss and on the projectile electron trajectories. In this case, a simple velocity vector addition model is sufficient for the determination of the kinematic effects. Thus, the velocity \mathbf{v} of the Auger electron in the laboratory frame is obtained by adding the projectile velocity \mathbf{V}_p to the velocity \mathbf{v}' of the electron in the projectile rest frame [2]. Denoting with prime, quantities in the projectile rest frame, the electron kinetic energy ε in the laboratory frame can be related to the corresponding rest frame electron kinetic energy ε' as:

$$\varepsilon = \varepsilon' + t_p + 2\sqrt{\varepsilon' t_p} \cos \theta' \quad (2.2)$$

or its more accurate relativistic counterpart

$$\varepsilon = \gamma_p \varepsilon' + t_p + \sqrt{(1 + \gamma') \varepsilon' (1 + \gamma_p) t_p} \cos \theta' \quad (2.3)$$

where $t_p = \frac{m}{M_p} E_p$ is the reduced projectile energy known also as the *cusp* electron energy (electrons isotachic to the projectile ion). E_p and M_p are the kinetic energy and mass of the projectile, respectively, while m is the electron mass and $\gamma_p (= 1 + \frac{t_p}{mc^2})$ and $\gamma' (= 1 + \frac{\varepsilon'}{mc^2})$ are the usual relativistic γ -parameters for speeds V_p and v' , respectively. Clearly, Eq. 2.3 can be seen to go to its classical limit Eq. 2.2, when γ_p and γ' go to 1.

At strictly zero degree observation ($\theta = 0^\circ$) the rest frame emission angle $\theta' = 0^\circ$ or 180° . Thus, as applicable to the ZAPS technique the relation between the electron kinetic energies in the laboratory ε and rest frame ε' can be written directly from Eq. 2.3 as:

$$\varepsilon(t_p, \varepsilon') = \gamma_p \varepsilon' + t_p \pm \sqrt{(1 + \gamma') \varepsilon' (1 + \gamma_p) t_p} \quad (2.4)$$

The \pm symbol represents the solution for either forward (+) or backward (-) emission from the ion. All our measurements to date correspond to the forward emitted electrons. The inverse of Eq. 2.4 can also be obtained for zero-degrees [6] to be:

$$\varepsilon'(t_p, \varepsilon) = \left[\sqrt{t_p \left(1 + \frac{\varepsilon}{2mc^2}\right)} - \sqrt{\varepsilon \left(1 + \frac{t_p}{2mc^2}\right)} \right]^2 \quad (2.5)$$

Once the values $i[j]$ (for each Auger calibration peak j) in the laboratory frame are measured directly from the raw spectrum, we may set $T_j(i) = \varepsilon_i$ and using a least three known Auger energies $\varepsilon'_j = EA_j$ ($j = 1, 2, 3$) the three calibration constants of Eq. 2.1 can be found applying a least squares fit solution using Eqs. 2.4:

$$\varepsilon(t_p, \varepsilon' = EA_j) = a + b \cdot i[j] + c \cdot i[j]^2 \quad (j = 1 \dots j_{max}) \quad (2.6)$$

$$S = \sum_{j=1}^{j_{max}} [\varepsilon'(t_p, \varepsilon(t_p, EA_j)) - EA_j]^2 \quad (2.7)$$

Thus, calibration parameters a, b, c are adjusted for fixed t_p until the sum S of the squares of the differences between the original EA_j and the calibrated Auger energies $\varepsilon'(t_p, \varepsilon(t_p, EA_j))$ has been minimized.

With this information available, the axis of the acquired spectrum can be transformed from channels i to laboratory energy in eV. Typically, this is done for the 5 ($j_{max} = 5$) main well known KLL Auger lines of Carbon given below in Table 1.

Table 1: Main KLL Auger lines of carbon used for calibration [3]. The laboratory energies are computed according to Eq. 2.4 for a carbon projectile energy of $E_p = 18$ MeV ($t_p = 822.87$ eV).

j	Auger line	Auger energy - EA (eV)	Lab energy - ε (eV)
1	$1s2s^2^2S$	227.17	1915.56
2	$1s2s2p^4P$	229.64	1922.73
3	$1s(2s2p^3P)^2P_-$	235.44	1939.45
4	$1s(2s2p^1P)^2P_+$	238.86	1949.26
5	$1s2p^2^2D$	242.15	1958.64

2.2 Laboratory to Rest frame Energy transformation

The previous procedure for calibration is not the only one available, and although it generates self-calibrating results it is not always accurate, since it ignores any possible errors of the projectile energy.

Once the energy in the lab frame is calibrated, which means that there is a defined relation between channels and laboratory frame, the spectrum is then transformed to the rest frame using Eq. 2.5.

2.3 Normalization

All previous procedures transform the x-axis of the spectrum, which is the energy axis. The following section describes the normalizations needed on the y-axis (N_{e_i} - the # of electrons counted in channel i to convert to Double Differential Cross Section ($DDCS_i$) given by the following equation [1]:

$$DDCS_i \equiv \frac{d^2\sigma_i}{d\Omega dE_i} = \frac{N_{e_i} DTC}{N_I L_{eff} n \overline{\Delta\Omega} \Delta E_i T \eta_i} \quad (2.8)$$

where i refers to the channel number of the PSD X projection.

Number of electrons recorded in channel i - N_{e_i}

This is the measurement taken from DAQ, which is the number of counted electrons in every channel i . The statistical uncertainty is $\delta N_{e_i} = \sqrt{N_{e_i}}$.

Dead-time correction - DTC

The DTC is defined as the ratio of total number of counts recorded by a scaler over the total number of counts recorded by the ADC. Basically it is an average correction for the case of an increased count rate that the DAQ cannot handle. The DAQ manufacturer claims a 1 MHz counting capability, therefore for a typical measurement with a count rate < 20 kHz, the DTC is considered to be 1 (i.e. no dead time). In principle this should be verified and we plan to do this in future measurements.

Number of ions - N_I

N_I is the number of ions collected on the DAQ Faraday Cup (FC2) during each spectrum measurement. It is given by the following formula:

$$N_I = \frac{Q(nC)}{q \cdot 1.6 \times 10^{-10}} \quad (2.9)$$

where q is the ion charge state, and $Q(nC)$ is the total charge recorded by FC2 and is calculated by the following formula:

$$Q(nC) = \frac{Q_{cnt} I_{FS}(nA)}{C_{nts}} \quad (2.10)$$

where Q_{cnt} is the number of counts set by the experimentalists, and equals the number of pulses generated from the BCI, and received by the DAQ. Once the requested number of pulses have been received, the measurement stops. I_{FS} is the maximum of the scale the BCI operates, typically measured in nA (usually 2, 6, 20 or 60 nA). Finally, C_{nts} is the rate of pulses generated by the BCI per second. For the Brookhaven BCI used for all measurements to date this is fixed at $C_{nts} = 100$ Hz.

The normalization of the total number of ion charge is based on the assumption that the beam current is not affected by collisions in the target.

Effective length of the gas-cell - L_{eff}

The effective length of the gas-cell. Typically, for a gas cell with actual length L_{gc} , with aperture openings of diameter D_1 and D_2 the effective length is given by $L_{eff} = L_{gc} + \frac{D_1 + D_2}{2}$. As explained in [7], the original gas cell apertures were widened. The effective length for all but the last measurement is given by $L = 50$ mm, $D_{entrance} = 1.5$ mm and $D_{exit} = 2.0$ mm to a total of $L_{eff} = 51.75$ mm. After the widening, the new values became: $D_{entrance} = 2.5$ mm and $D_{exit} = 2.5$ mm for a total of $L_{eff} = 52.50$ mm.

Target gas density - n

n is the number of molecules per cm^3 . Using the state equation, applicable to this range of pressures, and assuming that the gas temperature is at room temperature (300 °K), the density can be calculated by the following formula [1]:

$$n (\# \text{ molecules}/\text{cm}^3) = 3.222 \times 10^{13} P(\text{mTorr}) \quad (2.11)$$

$\overline{\Delta\Omega}$

$\Delta\Omega_0$ is the *point source* solid angle defined by the opening of the lens entrance ($d_{LE} = 4.0$ mm) and the distance of the lens entrance to the center

of the gas cell ($l_{dist} \approx 289$ mm).

$$\Delta\Omega_0 = \frac{\pi d_{LE}^2}{4 l_{dist}^2} = 1.505 \times 10^{-4} \text{ sr.} \quad (2.12)$$

A small correction gives the solid angle averaged over the length of the gas cell $\overline{\Delta\Omega}$ giving $\overline{\Delta\Omega} = 1.00664 \Delta\Omega_0 = 1.515 \times 10^{-4}$ sr.

ΔE

ΔE is the energy step of the spectrum per channel and is obtained from the first derivative of Eq. 2.1 with respect to the channel number leading to:

$$\Delta E_i = b + 2c \cdot i \quad (2.13)$$

It is the only correction that has a non-uniform effect across the PSD as it increases with i .

Analyser transmission - T

T is defined as the transmission of the spectrograph assumed here to be independent of channel number. It is defined as the ratio of the number of particles reaching the detector to the number of particles entering the spectrograph (i.e. the entry lens). This can in principle also depend on the specific transmission of the lens itself and therefore depend on the lens voltages and also the retardation factor F [8]. However, as already shown in Ref. [1] (Fig. 46) for F -values up to 8 this was found to be a constant and therefore independent of the lens voltages. Thus, the transmission was determined by the three grids of 90% transmission leading to a total of $T = 0.90^3 = 0.729\%$ transmission. We note that active area of the PSD was seen to be from channel 40 up to 220, in the case of a 256×256 DAQ counts matrix.

MCP efficiency - η

η is the MCP efficiency. It is the probability that an electron that reaches the surface of the MCP will create a measurable signal. The efficiency of the MCP's depends on the active area of the MCP, and the energy of the electrons, presenting its maximum efficiency at around 300 to 350 eV. To ensure an effective efficiency over the active PSD area, the whole MCP system is biased appropriately so that the central trajectory electrons always imping on the front MCP at an energy of 1000 eV as described in detail in Ref. [1]. Determination of the efficiency η can be done either by comparison to Binary Encounter electron measurements [5] or using known cross sections for the production of target Auger electrons. To date we have not really needed any absolute DDCS calibrations since we have been primarily interested in

the ratio of Auger lines, i.e. relative measurements. However, a preliminary test using known Ne KLL Auger spectra using a 3 MeV proton beam showed the overall efficiency $\bar{\eta} = 35\%$ which was considered satisfactory.

3 Data analysis

3.1 Homebuilt Software

3.1.1 Self Energy Calibrating Excel

Most of the data analysis have been successfully integrated in an Excel™ calculation sheet. All it requires from the user is:

- The projection file that is generated from the DAQ [9].
- A fit of the raw spectra, mainly to obtain the peak centers and background.
- Experimental parameters such as beam energy, BCI counts [10], gas pressure etc.

Provided with these data, it performs the following procedures:

1. Using the relativistic energy transformation equations (see Energy calibration above) along with established Auger electron standards and using the centers of the fitted peaks, it calculates the calibration constants a, b, c (as discussed above) providing the laboratory energy calibration in eV.
2. It subtracts a fitted quadratic background from the raw data.
3. It kinematically transforms the spectra from the laboratory frame to the rest frame [1].
4. It calculates an overall scaling factor containing all the coefficients of equation 2.8 except the ΔE_i , and finally produces the DDCS for the given spectrum.

3.1.2 Optimal Slit settings Excel

This is an excel worksheet that calculates the optimal openings of Slits 1 and 2 in our beam line, for highest transmission of the ion beam through the apertures of the gas cell [7], the entrance of the lens and finally the exit of the lens. Based on simple geometrical arguments, it calculates the portion of the ion beam that falls on every aperture, therefore it is used to maximize the ion transmission by simultaneously minimizing the “noise” generated by ions hitting the gas cell.

3.1.3 Spectrograph voltage Excel

This is an Excel spreadsheet that calculates all necessary voltages that need to be applied to the HDA and the lens for proper operation as function mainly of the central energy W and retardation factor F . It is used to manually set the voltages or cross check the values set by the automatic voltage control unit supplied by Fasmatech's control hardware and software.

3.1.4 Various other control programs

Other than the above, there are minor LabVIEW programs, that were developed for testing various pieces of equipment, or subroutines to customize the operation of the Fasmatech functions. A software counter was built to test signal from the BCI unit. Various calibration schemes for the power supplies were also developed.

3.2 Results using SIMION software

SIMION [11] is a software package primarily used to calculate electric fields and the trajectories of charged particles in those fields for a given configuration of electrodes with voltages and particle initial conditions. SIMION is used extensively in the APAPES project to model various electrostatic electrode setups. The following is a brief list of the abstracts of publications in which Lua programs for SIMION were used.

3.2.1 Experimental energy resolution of a paracentric hemispherical deflector analyzer for different entry positions and bias

A specially designed hemispherical deflector analyzer (HDA) with 5-element input lens having a movable entry position R_0 suitable for electron energy analysis in atomic collisions was constructed and tested. The energy resolution of the HDA was experimentally determined for three different entry positions $R_0 = 84, 100, 112$ mm as a function of the nominal entry potential $V(R_0)$ under pre-retardation conditions. The resolution for the (conventional) entry at the mean radius $R_0 = 100$ mm was found to be a factor of 1.6-2 times worse than the resolution for the two (paracentric) positions $R_0 = 84$ and 112 mm at particular values of $V(R_0)$. These results provide the first experimental verification and a proof of principle of the utility of such a paracentric HDA, while demonstrating its advantages over the conventional HDA: greater dispersion with reduced angular aberrations resulting in better energy resolution without the use of any additional fringing field correction electrodes. Supporting simulations of the entire lens plus HDA spectrometer are also provided and mostly found to be within 20% 30% of experimental values. The paracentric HDA is expected to provide a lower

cost and/or more compact alternative to the conventional HDA particularly useful in modern applications utilizing a position sensitive detector [12].

3.2.2 Determination of the solid angle and response function of a hemispherical spectrograph with injection lens for Auger electrons emitted from long lived projectile states

SIMION 8.1 Monte Carlo type simulations of the response function and detection solid angle for long lived Auger states (lifetime $\tau \approx 10^9 - 10^5$ s) recorded by a hemispherical spectrograph with injection lens and position sensitive detector used for high resolution Auger spectroscopy of ion beams are presented. Also included in these simulations for the first time are kinematic effects particular to Auger emission from fast moving projectile ions such as line broadening and solid angle limitations allowing for a more accurate and realistic line shape modeling. Results are found to be in excellent agreement with measured electron line shapes of both long lived $1s2s2p^4P$ and prompt Auger projectile states formed by electron capture in collisions of 25.3 MeV F^{7+} with H_2 and 12.0 MeV C^{4+} with Ne recorded at 0° to the beam direction. These results are important for the accurate evaluation of the $1s2s2p^4P / ^2P$ ratio of K-Auger cross sections whose observed non-statistical production by electron capture into He-like ions, recently a field of interesting interpretations, awaits further resolution [2].

3.2.3 The Optimization of a 4-Element Input Lens on a Hemispherical Deflector Analyzer Using SIMION

Code was developed for the simulation procedure for finding the optimal voltages of an input lens used for high resolution Auger projectile electron spectroscopy at the new atomic physics experimental station located at the 5 MV Tandem Accelerator of the INPP at NCSR “Demokritos” [13]. The station consists of a hemispherical deflector analyzer (HDA) with a 4-element injection lens and 2-D position sensitive detector (PSD) to be used for studies of projectile excitation processes in energetic ion-atom collisions. The optimization was performed by simulations using the SIMION 8.1 package [11], [14].

3.2.4 Voltage optimization of a 4-element injection lens on a hemispherical spectrograph with virtual entry aperture

We present simulation results for a biased paracentric hemispherical deflector analyzer equipped with a 4-element input lens and a position sensitive detector used in our zero-degree Auger projectile spectroscopy apparatus. Calculations of electron trajectories traversing the lens and analyzer fields were performed and cross checked using both boundary-element and finite-difference methods. The two middle lens electrode voltages were varied as

free parameters, while various criteria were used to select their optimal values in an effort to obtain improved energy resolution [15].

3.2.5 Evaluation of the effective solid angle of a hemispherical deflector analyser with injection lens for metastable Auger projectile states

The accurate determination of the electron yield of a metastable projectile Auger state necessitates the careful evaluation of the corresponding effective solid angle, i.e. the geometrical solid angle convoluted with the decay time of the metastable state. Recently [2], a SIMION Monte Carlo type simulations of the effective solid angle for long lived projectile Auger states (lifetime $\tau \approx 10^9 - 10^5$ s) recorded by a hemispherical spectrograph with injection lens and position sensitive detector in the direction of the projectile ion was presented. These results are important for the accurate evaluation of the $1s2s2p^4P / ^2P$ ratio of K-Auger cross sections whose observed non-statistical production by electron capture into He-like ions, recently a field of interesting interpretations, awaits final resolution. Here we expand and systematize our investigation using the same techniques to expose universal behaviors of the effective solid angle covering life-times of $1s2s2p^4P$ states for all first row ions. Our results are also compared to purely geometrical calculations of the solid angle that omit the lensing effects and serve as a benchmark for a deeper insight into the effect [16].

4 Presentation of new results

4.1 Capture ratio R

Most of our results have already been published and/or presented in international conferences (see also Work Package 10). One of the main objectives is the determination of the experimental ratio $R = ^4P / ^2P$ for capture at various projectile velocities. In Fig. 1 are preliminary results presented at CDAMOP 2015 [17].

Future plans include more measurements over the full energy range (0.5 MeV/u - 1.5 MeV/u) using all 4 gas targets (H₂, He, Ne, Ar). Of great importance will be measurements using practically pure ground state C⁴⁺ beam that will be available as soon as the terminal gas stripper installation is finalized.

4.2 Biased gas cell measurements

The biased gas-cell technique [19] has already been presented and discussed in WP 8. It will be an important tool in future measurements.

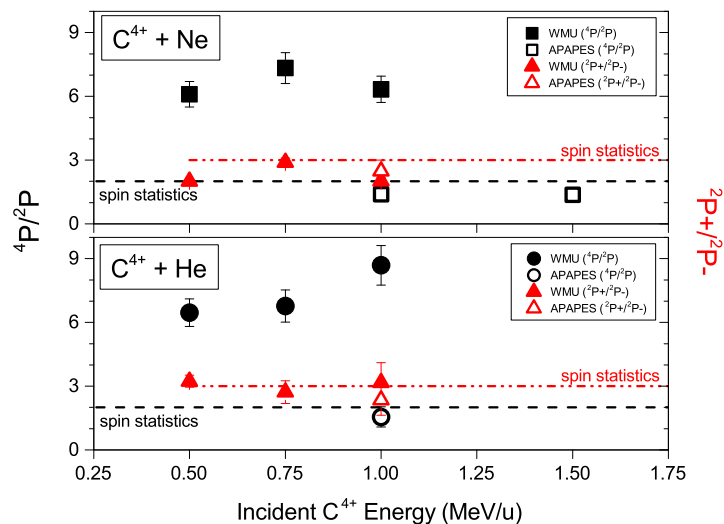


Figure 1: : Experimentally determined ratios (left scale) for $R = {}^4 P/{}^2 P$ and (right scale in red) for $R = {}^2 P_+ / {}^2 P_-$. Also shown for comparison are the results of the previously published experimental data from Ref. [18]. Corrections for both the $1s2s2p {}^4 P$ life time effects and TE have also been included. Adapted from Fig. 3 of Ref. [17].

5 Concluding Remarks

In pursuing our measurements towards the eventual goal of the APAPES initiative, we have presented interesting new results concerning the Li-like KLL Auger spectra produced in 9, 12 and 18 MeV collisions of C^{4+} ions on various gases. The implementation of the gas and foil post strippers also was also successfully completed. Both foil and gas post stripper significantly extend the high charge state capabilities of the Demokritos tandem.

Our results to date have been mostly presented at international meetings as well as articles in international journals. In Work Package 10 all dissemination means are presented. However, many more new results are expected to be published in the near future. The field of Zero-degree Auger projectile spectroscopy (ZAPS) is a very rich field of investigation and the APAPES project will continue this initiative even after the end of the THALES granting period (30/11/2015) in the hope of also soon attracting future support.

Acknowledgements

This research has been co-financed by the European Union (European Social Fund-ESF) and Greek national funds through the Operational Program “Education and Lifelong Learning” of the National Strategic Reference Framework (NSRF) Research Funding Program: THALES. Investing in knowledge society through the European Social Fund, grant No MIS 377289.

References

- [1] E. P. Benis, Ph.D. dissertation, Dept. of Physics, University of Crete, 2001, (unpublished).
- [2] S. Doukas *et al.*, Review of Scientific Instruments **86**, 043111 (2015).
- [3] R. Bruch, K. T. Chung, W. L. Luken, and J. C. Culberson, Phys. Rev. A **31**, 310 (1985).
- [4] N. Stolterfoht, Phys. Rep. **146**, 315 (1987).
- [5] T. J. M. Zouros and D. H. Lee, in *Accelerator-based atomic physics techniques and applications*, edited by S. M. Shafroth and J. C. Austin (American Institute of Physics Conference Series, Woodbury, NY, 1997), Chap. 13, pp. 426–479.
- [6] K. Kawatsura *et al.*, Nucl. Instrum. Methods Phys. Res. B **48**, 103 (1990).
- [7] http://apapes.physics.uoc.gr/work_package_5.php
- [8] T. J. M. Zouros and E. P. Benis, Appl. Phys. Lett. **86**, 094105 (2005).
- [9] http://apapes.physics.uoc.gr/work_package_6.php
- [10] <http://www.ni.com/pdf/manuals/371931f.pdf>
- [11] <http://www.simion.com>
- [12] M. Dogan, M. Ulu, G. G. Gennarakis, and T. J. M. Zouros, Review of Scientific Instruments **84**, 043105 (2013).
- [13] <http://apapes.physics.uoc.gr>
- [14] T. J. M. Zouros *et al.*, Microscopy and Microanalysis **21**, 148 (2015).
- [15] G. Martínez *et al.*, Nuclear Instruments and Methods in Physics Research Section B: Beam Interactions with Materials and Atoms (2015).

- [16] E. Benis *et al.*, Nuclear Instruments and Methods in Physics Research Section B: Beam Interactions with Materials and Atoms **365**, 457 (2015).
- [17] A. Dimitriou *et al.*, in *Proceedings of CDAMOP 2015: 4th International Conference on Current Developments in Atomic and Optical Physics with Applications* (Journal of Atomic, Molecular, Condensate and Nano Physics, India, 2015), Vol. xxx, pp. xx-xx.
- [18] D. Strohschein *et al.*, Phys. Rev. A **77**, 022706 (2008).
- [19] I. Madesis *et al.*, J. Phys: Conf. Ser. **635**, 052082 (2015).